International Journal of Heat and Mass Transfer 168 (2021) 120842

Contents lists available at ScienceDirect

International Journal of Heat and Mass Transfer

journal homepage: www.elsevier.com/locate/hmt

Temperature-depended ion concentration polarization in electrokinetic energy conversion

Rui Long*, Fan Wu, Xiyu Chen, Zhichun Liu*, Wei Liu

School of Energy and Power Engineering, Huazhong University of Science and Technology, Wuhan 430074, PR China

ARTICLE INFO

Article history:
Received 27 October 2020
Revised 6 December 2020
Accepted 16 December 2020

Keywords:
Electrokinetic energy conversion
Ionic current source
Temperature
Membrane thermal conductivity
Nanofluidics

ABSTRACT

Previous studies on the electrokinetic energy conversion (EKEC) are limited to the isothermal condition at the environmental temperature. Here effects of temperature and membrane thermal conductivity are systematically investigated. Under isothermal conditions, elevated temperature can improve the electric power while the energy efficiency stays unchanged. Under non-isothermal conditions, at small membrane thermal conductivities, a negative temperature difference contributes to the electric power for dramatically enhanced streaming current as enhanced ion mobility along the streaming direction induces an internal ion concentration polarization (IICP) that generates a co-flow concentration gradient in the nanopore interior. At large membrane thermal conductivities, the positive temperature difference reverses the external ion concentration polarization (EICP) in the solution reservoirs due to the Soret effect, resulting in more obvious electric power improvement. Furthermore, a criterion to enhance the EKEC performance via employing asymmetric temperatures is proposed, and an alternative way to construct the tunable ionic current source is presented. Present study provides guidance for enhancing the EKEC performance by employing waste heat, and fabricating nanofluidic functional devices.

© 2020 Elsevier Ltd. All rights reserved.

1. Introduction

Advances in nanotechnology and nanofabrication contribute to constructing high performance nanofluidic electrokinetic energy conversion (EKEC) devices for harvesting the vibrational energy and hydrostatic energy powered by solar or waste-heat, thus to relieve the vast energy consumption and the induced escalating environment issues [1]. In the charged nanochannel that attracts counter ions and repels co-ions, an electric double layer (EDL) is formed adjacent to the nanochannel wall. When the Debye length, characterizing the EDL thickness, is comparable with the nanochannel size, significant charge separation is established in the nanochannel interior, leading to access counter ions [2–4]. In the EKEC process, an external pressure difference is applied across the charged nanochannel, producing a streaming flow that drags the access counter ion and offers a streaming current, which could be employed to drive an external load [5–7].

Efforts regarding the EKEC mainly focus on improving the energy conversion efficiency via developing appropriate nanochannel geometries [8–11], employing Newtonian/non-Newtonian fluids [12] and various salt types [13,8], tuning solution pH [14], as well as modifying membrane surface properties [15–17]. For short nanochannels, strong ion concentration polarization (ICP) exists, and the inter-pore ionic movement is affected by the ion depletion/accumulation around the pore ends [18]. The ionic conductance can be impacted by the external applied pressure and the streaming flow convection [19,20]. Xie et al. [21] obtained an efficiency of 5% in single track-etched nanopores with small radii of 31 nm. Recently, hydrodynamic slip is employed to enhance the energy conversion efficiency [18,22–25]. Hydrodynamic slippery reduces energy dissipated by viscous dissipation and the electrical resistance of the nanopore. Yan et al. [26] measured an energy efficiency of 35% at a slip length of about 30 nm. Chang and Yang [27] predicted the energy efficiency can be greatly improved to above 40% when the slip ratio is greater than 0.7. Furthermore, Mei et al. [28] added buffer anions into the salt solutions, and found that the power density can be enhanced as high as 1.5-26 times for increased space charge density of mobile ions. The energy conversion efficiency of the EKEC system via a Nafion membrane together with an aqueous LiI/I_2 redox can reach up to 14% [29]. Liu et al. [30] fabricated a flexible microfluidics electrokinetic conversion nanogenerator, and a pulse voltage of 1.5 V and current of 1 μA were obtained. Haldrup et al. [31] reported an EKEC efficiency larger than 35% through the charged polymeric membrane synthesized from blends of nitrocellulose and sulfonated polystyrene. By choosing moderate ion exchange capacity and ap-

* Correspondence authors.
E-mail addresses: r_long@hust.edu.cn (R. Long), zcliu@hust.edu.cn (Z. Liu).

https://doi.org/10.1016/j.ijheatmasstransfer.2020.120842
0017-9310/© 2020 Elsevier Ltd. All rights reserved.

propriate pore diameter, a remarkably large EKEC efficiency of 46% was achieved [32].

However, previous studies on the EKEC process are limited to the isothermal operating condition [6]. The operating temperature is often maintained at the environmental temperature. The effects of operating temperature variation on the system performance have been never considered. Furthermore, with temperature gradient imposed across the nanopore, ions tend to mitigate from the hot/cold side to the other side due to its intrinsic response to the temperature gradient due to the Soret effect [33–35]. Long et al. [36,37] investigated the concentration gradient ion transportation and energy conversion under asymmetric temperature differences in thermally insulated nanochannel, and found that a counter-diffusion temperature gradient can promote the selectivity and suppresses the ICP, resulting in enhanced membrane potential and electric power. In previous literatures, the nanochannel is treated as ideally thermally insulated, and the Soret effect plays negligible roles compared to that of temperature depended physical properties, especially the temperature depended ion mobility [35–38]. The material thermal conductivity for fabricating nanopores can reach a hundred W/(m•K) [39]. When temperature gradient imposed, heat transfer occurs both in the liquid solution and solid membrane. The trans-channel solution temperature distribution is impacted by the membrane thermal conductivity. Long et al. [40] further investigated the effects of the membrane thermal conductivity on the nanofluidic salinity gradient energy conversion, and proposed a criterion for membrane selection based on membrane thermal conductivities. Mai et al. [41] experimentally achieved a 64% improvement of power generation at a temperature of 25 K. In addition, Ghonge et al. [42] found that the pressure driven streaming flow can be suppressed or enhanced due to the Soret effect and the nature of the electrolyte.

Since the ionic current in the EKEC is mainly determined by the access charges dragged by the streaming flow, the operating temperature could impact the EKEC performance for the temperature depended physical properties and ionic temperature response. Research on temperature-depended electrokinetic energy conversion is highly demanded. In present study, the electrokinetic energy conversion performance under isothermal and non-isothermal conditions are systematically evaluated. The temperature-depended internal ion concentration polarization and external ion concentration polarization are analyzed. A criterion to enhance the electrokinetic energy conversion performance via employing asymmetric temperatures is presented. Furthermore, an alternative application originating from the system response to the asymmetric temperature difference is proposed. Understanding the thermally electrokinetic energy conversion provides guidance for enhancing the electrokinetic energy conversion by employing waste heat, and fabricating nanofluidic functional devices.

2. System description

As depicted in Fig. 1, we consider a single pore membrane with radius $R_n = 20$ nm, and length $L_n = 1000$ nm, which separates two reserviors at different temperatures. The surface charge density of membrane surface is fixed at σ =-0.1 C/m^2. The reserviors (radius $R_r = 1000$ nm and length $L_r = 1000$ nm) are filled with KCl solutions whose concentration varies from 10^{-2} mM to 10^3 mM. And an external pressure (1MPa) is applied on the end of the left reservior. T_L and T_R denotes the temperature of the left/right reservior.

The Poisson-Nernst-Planck equations, Navier-Stokes equations and energy conservation equation are employed to illustrate the

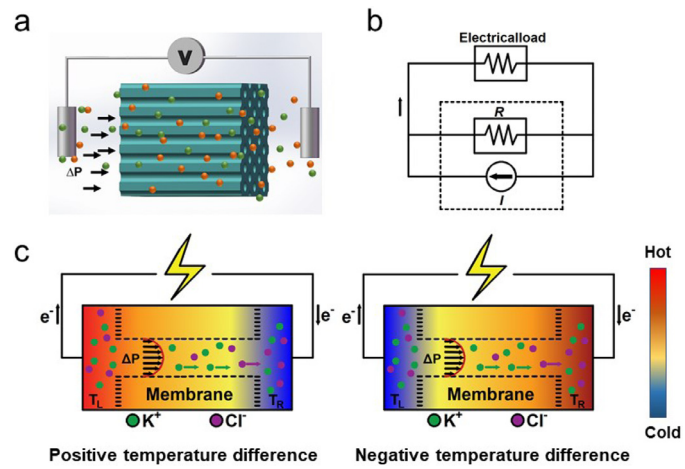

Fig. 1. (a) Schematic diagram of the nanofluidic electrokinetic energy conversion. (b) Schematic circuit diagram of the nanofluidic electrokinetic energy conversion system. (c) Schematic illustration of the temperature and ion concentration profiles under the positive temperature difference (PTD, $T_L > T_R$) and negative temperature difference (NTD, $T_L < T_R$), where T_L and T_R denote the temperature of the left/right reservior.

ion transportation and flow characteristics [35,38,40]

$$-\nabla \cdot (\varepsilon \nabla \phi) = F \sum_{i=1}^{2} z_i c_i \tag{1}$$

$$\nabla \cdot \boldsymbol{J}_i = 0, \text{ where } \boldsymbol{J}_i = c_i \boldsymbol{u} - D_i \nabla c_i - \frac{D_i z_i F c_i}{RT} \nabla \phi - \frac{2 D_i \alpha_i c_i}{T} \nabla T \tag{2}$$

$$-\nabla p + \nabla \cdot (\mu \nabla \boldsymbol{u}) - F \sum_{i=1}^{2} z_i c_i \nabla \phi - \frac{1}{2} |\nabla \phi|^2 \nabla \varepsilon = 0 \tag{3}$$

$$\nabla \cdot \boldsymbol{u} = 0 \tag{4}$$

$$\rho C_p \boldsymbol{u} \cdot \nabla T = \nabla \cdot (k_l \nabla T) \text{ for the liquid zone} \tag{5}$$

$$\nabla \cdot (k_s \nabla T) = 0 \text{ for the solid membrane} \tag{6}$$

where ϕ is the electrical potential. $\boldsymbol{J}_i$, c_i,$D_i$and $z_i$are the ionic flux, concentration, diffusivity, and valence of the ith ionic species, respectively ($i = 1$ for K^+ and $i = 2$ for Cl^-). α_i is the reduced Soret coefficient. α=0.5 for K^+ and α= 0.1 for Cl^- [43]. F, R and T are the Faraday constant, universal gas constant and the fluid temperature. ε, p, and $\boldsymbol{u}$are the permittivity, pressure, and velocity of the fluid. ρ,C_p,and k are the density, specific capacity, and thermal conductivity. The subscript s is for the solid membrane and l is for the liquid zone. The temperature-depended properties can be seen in Appendix A1. Eqs. (1)–(6) can be solved with proper boundary conditions [40]. The calculation is conducted via the commercial multiphysics software COMSOL based on the finite element method with finned quadrilateral meshes to guarantee that calculation data are completely converged and mesh independent. The validity of the numerical model employed in present study can be found in our previous studies [8,37,40].

The electric current is calculated by $I = \int_\Lambda F(\sum_{i=1}^{2} z_i \boldsymbol{J}_i) \cdot \boldsymbol{n} d\Lambda$, where $\boldsymbol{n}$ is the normal vector Λ represents the reservoir end. The I-V characteristics of the nanofluidic electrokinetic energy conversion system under isothermal and non-isothermal conditions can be seen in Fig. A1, which present an Ohm-like behavior. Based on its equivalent circuit, the streaming current (I_{str}) can be obtained under the short circuit condition. And the internal electric resistance

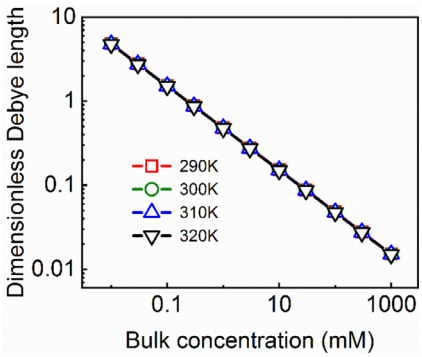

Fig. 2. Dimensionless Debye length under various bulk concentration. The Debye length is normalized by the channel radius fixed at 20nm.

(R_{str}) is calculated from the curve slop. The energy conversion system achieves its maximum power $P_{max} = I_{str}{}^2 R_{str}\ /4 = I_{str}E_{str}/4$, when the output voltage is half of the streamming potential $E_{str}= I_{str}\ R_{str}$. The energy conversion efficiency at the maximum power is calculated as [8]

$$\eta_{\max} = \frac{P_{\max}}{\Delta pQ_{\max,P}} = \frac{I_{str}{}^2 R_{str}}{4\Delta pQ_{\Delta V=0.5E_{str}}} \tag{7}$$

where Q denotes the corresponding transmembrane streaming flow rate.

3. Results and discussion

3.1. Performance under isothermal conditions

We first investigate the EKEC performance under the isothermal conditions where the operating temperature varies from 290 K to 320 K. The transmembrane ion transportation significantly depends on the electric double layer (EDL) overlapping degree. The thickness of the EDL can be characterized by the Debye length $\lambda_D = \sqrt{\varepsilon RT/2F^2c_0}$[44] . Here the Debye length normalized by the channel radius under various operating temperature is presented in Fig. 2. As shown in Fig. 3, at low bulk concentrations, although the EDL overlapping degree is significant, the access charge is still less for very low ion concentration. As the concentration increases, access ions dragged by the streaming flow are augmented, resulting in increased streaming current. At high concentrations, the EDL is much thinned, charges could not be effectively separated, leading to decreased access charge and streaming current. As depicted in Fig. 4, higher temperature significantly contributes to the streaming flow thus the streaming current. The concentration profiles under various operating temperatures do not exhibit much difference. Therefore, the electric resistance is mainly impacted by the ionic mobility. The higher temperature, the larger ionic mobility, thereby decreased electric resistance. The variation of the electric resistance is relatively less compared to the increase of the streaming current, leading to upgraded electric power at elevated operating temperatures. The energy conversion efficiency is insensitive to the operating temperature due to simultaneously enhanced streaming flow and electric power, as depicted in Fig. 3.

We further investigate the impact of the channel radius on the EKEC performance. Fig. 5 presents the normalized streaming current electric power under different normalized channel radius at various operating temperature. In the studied range of the channel radius, the streaming current increases with increasing channel radius for enhanced transmembrane streaming flowrate at larger channel size. The electric power also presents a positive dependence on the channel radius for augmented streaming current. Higher operating temperature leads to larger streaming current and upgraded electric power, as shown in Fig. 5.

3.2. Performance under non-isothermal conditions

Here we focus on the effects of the transmembrane temperature difference on the EKEC process. Varied membrane thermal conductivities are considered, which covers common membrane materials such as polyethylene terephthalate (k = 0.15 W·m^{-1}K^{-1}), alumina (k = 30 W·m^{-1}K^{-1}), and the silicon nitride (k = 120 W·m^{-1}K^{-1}). We name the positive temperature difference as that the temperature gradient is same direction with the pressure gradient. And the negative temperature difference is denoted as the opposite situation. IT, PTD, and NTD represent the isothermal conditions ($T_L = T_R$ = 290 K), positive temperature difference (T_L = 320 K, T_R = 290 K) and negative temperature difference (T_L = 290 K, T_R = 320 K), respectively. As shown in Fig. 6, both negative and positive temperature difference contribute to the streaming current due to enhanced streaming flowrate. At small bulk concentrations, the EDL overlapping degree is significant. The ion distribution in the nanopore interior is governed by the electrostatic force, and is independent of the bulk concentration. The impacts of the Soret effect in the nanopore interior can be neglected. As shown in Fig. 7, the axial cation concentration profiles with/out considering the Soret effect the in the nanopore interior stay almost unchanged. At small membrane thermal conductivities, the temperature gradient in the nanopore interior is much prevailing (Fig. A2 in the Appendix). The ion mobility increases along the flow direction, which contributes to ion transportation from the nanopore interior to the nanopore exit, leading to ion depletion at the exit section. An internal ion concentration polarization (IICP) is formed, generating a concentration gradient along the flow direction that provides an additional diffusion current in the flow direction and results in augmented streaming current. Under the positive temperature difference, the solution temperature is decreased along the flow direction. The ion mobility decreases along the flow direction, leading to ion aggregation near the nanopore exit and the formation of the internal ion concentration polarization that produces a counter-flow concentration gradient, which is adverse to the streaming current enhancement.

At large thermal conductivities, the internal ion concentration polarization is suppressed due to uniformed temperature distribution in the nanopore interior. And the external ion concentration polarization (EICP) in the solution reservoir begins to act dominantly, where the ion depletion/aggregation occurs in the left/right reservoirs, which hinders the trans-pore ion transportation. Large thermal conductivity induces strong temperature gradient in the reservoir, leading to significantly suppressed/enhanced ion depletion in the nanopore entrance due to the Soret effect under the positive/negative temperature difference (Fig. 7). Therefore, the streaming current under the positive temperature difference overrides that under the negative one. At high bulk concentrations, the EDL is much thinner, and the electrostatic force is weak. Effective local concentration gradient cannot be established in the nanopore interior. At large thermal conductivities, the reversed EICP is established, where ion aggregation/depletion occurs in the nanopore entrance/exit under the positive temperature difference, which induces a transmembrane concentration difference along the flow direction that contributes to ion diffusion and the ionic current (Fig. 7d). A negative temperature induces a transmembrane concentration difference against the flow direction that deteriorates the ionic current (Fig. A3 in the Appendix).

Figs. 6d-f depict the electric resistance under different temperature differences and membrane thermal conductivities. At low concentrations, the ion distribution is independent of the bulk concentration due to significant EDL overlapping degree in the nanopore

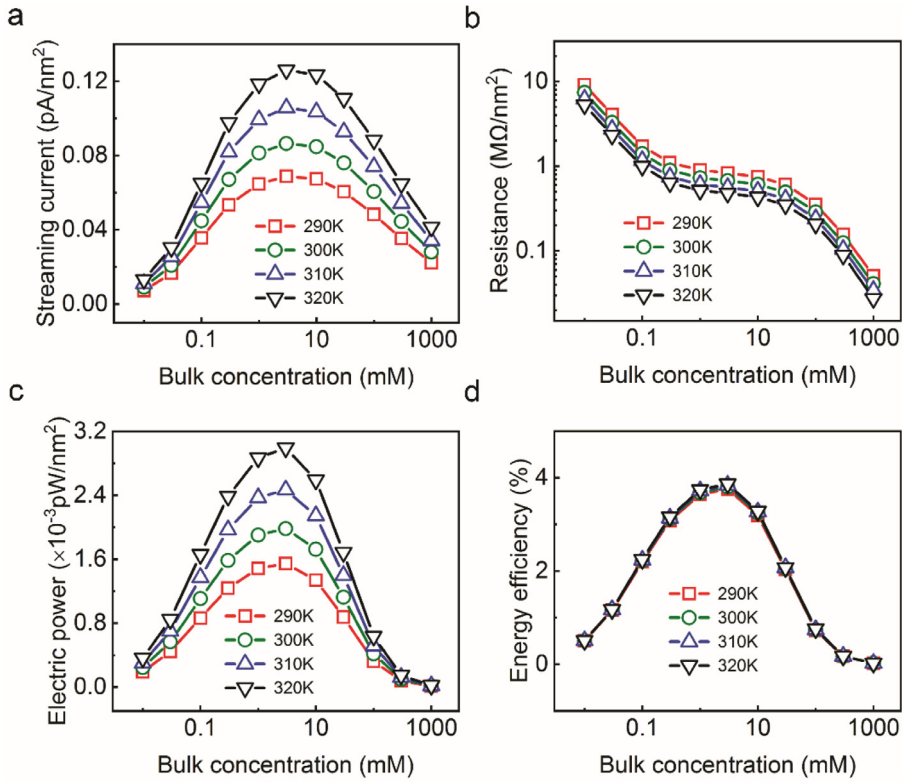

Fig. 3. (a) Streaming current, (b) resistance, (c) electric power, and (d) energy efficiency under various bulk concentrations and operating temperatures. The streaming current, resistance and the electric power are nomarlized by the cross sectional area. In the calculation, the channel radius is 20nm.

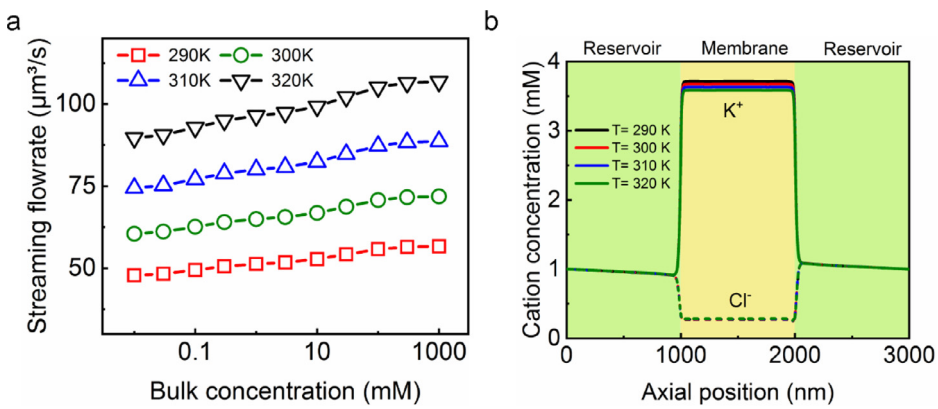

Fig. 4. (a) Streaming flowrate under different bulk concentrations and operating temperatures; (b) Axial concentration under different operating temperaures where the bulk concentration is 1 mM. In the calculation, the channel radius is 20nm.

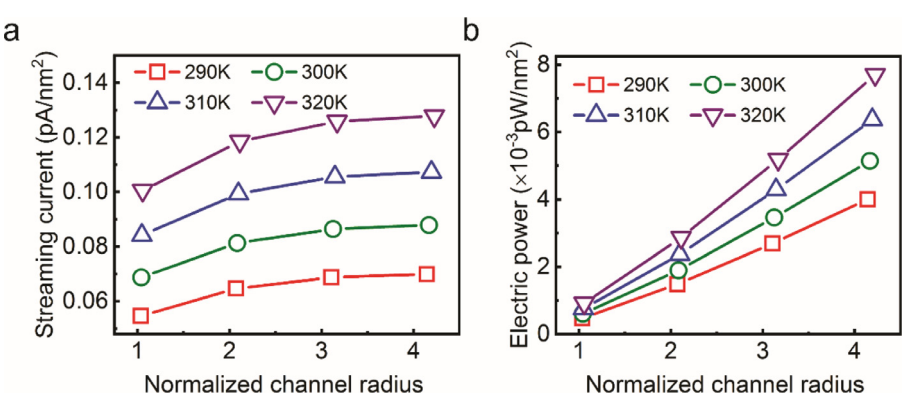

Fig. 5. (a) Streaming current, (b) electric power under different channel radius at various operating temperature. The streaming current and the electric power are normalized by the cross sectional area. The channel radius is normalazed by the Debye length. In the calcualtion, the bulk concentration is 1 mM.

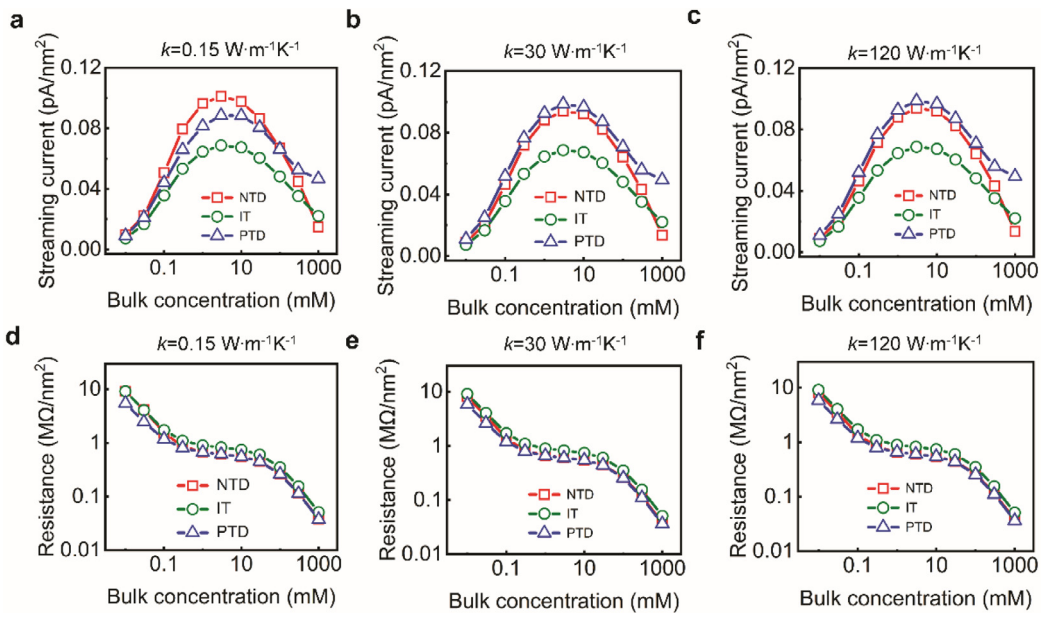

Fig. 6. Streaming current and electric resistance under different transmembrane temperature differences, (a, d) k=0.15 W•m^{-1}K^{-1}; (b, e) k=30 W•m^{-1}K^{-1}; (c, f) k=120 W•m^{-1}K^{-1}. The streaming current and resistance are normalized by the cross sectional area. In the calculation, the channel radius is 20nm.

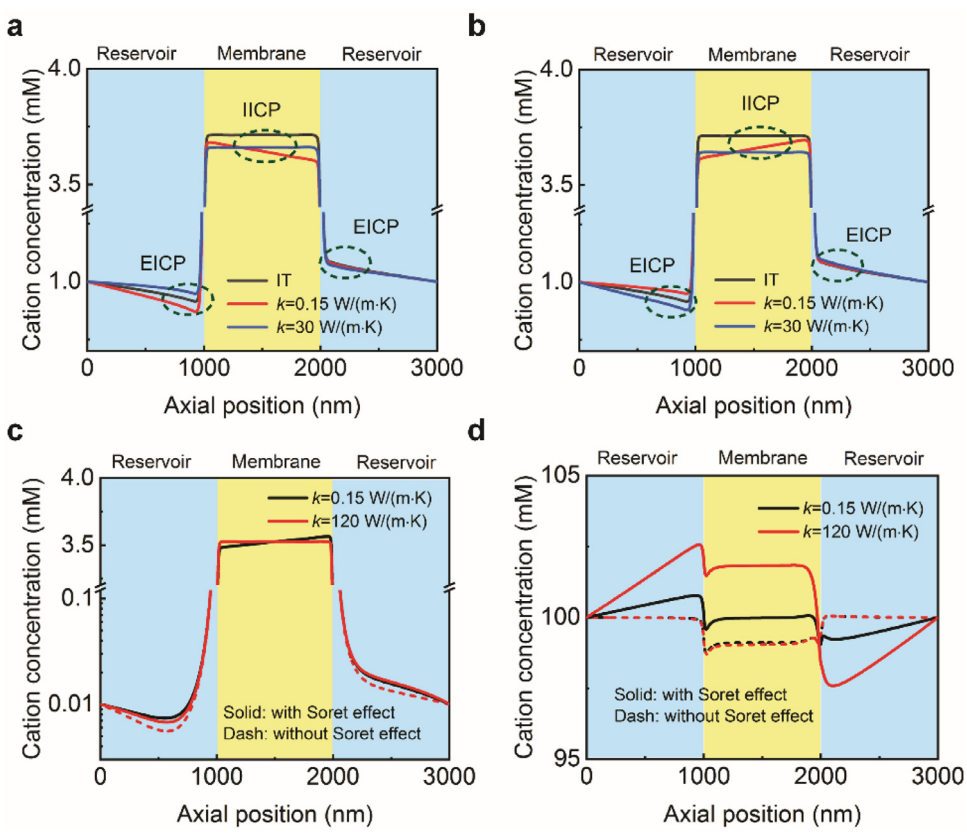

Fig. 7. Cation concentration profiles under the NTD (a) and PTD (b) for different membrane thermal conductivities at the bulk concentration of 1 mM; (c, d) Cation concentration profiles under the PTD at low/high bulk concentration (0.01 mM and 100 mM) with/out considering the Soret effect. In the calculation, the channel radius is 20nm.

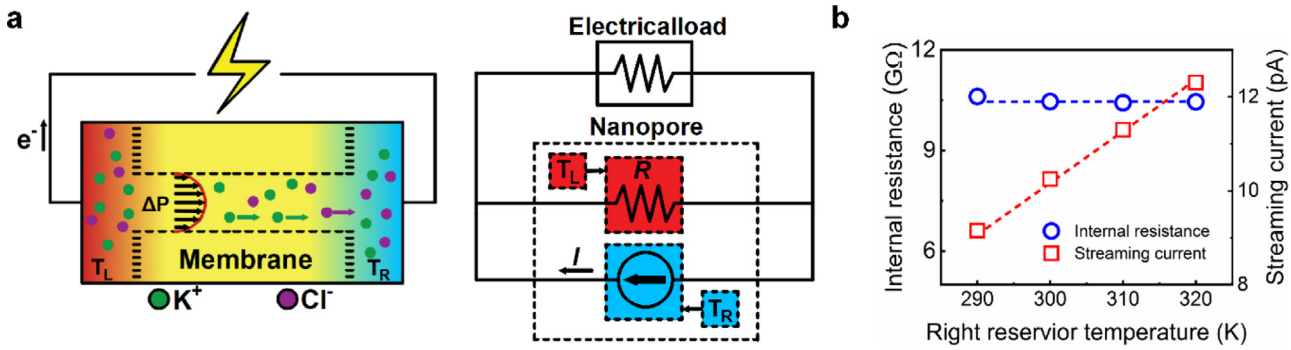

Fig. 8. (a) Schematic diagram of the tunable ionic current source. (b) Internal resistance and streaming current under various right reservoir temperatures for a PET membrane (k=0.15 W•m^{-1}K^{-1}). In the calculation, the left servitor temperature is 290 K. And the channel radius is 20nm.

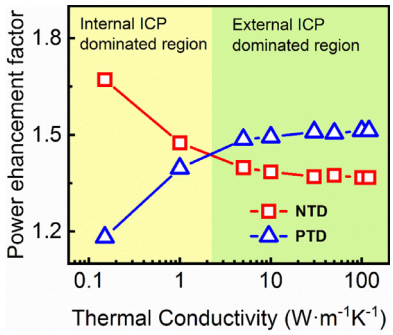

Fig. 9. Power enhancement factor with different membrane thermal conductivities. The power enhancement factor is defined as the power under the IT condition divided by that under the NTD or PTD. In the calculation, the channel radius is 20nm, and the bulk concentration is 1 mM.

interior, and the transmembrane ion transportation is determined by the mobility of the ions at the entrance mouth. Therefore, at low concentrations, the electric resistance under the negative temperature difference nearly coincides with that under the isothermal conditions. Under the negative temperature difference, higher solution temperature is applied at the entrance mouth, leading to decreases electric resistance. At high bulk concentrations, the ion distribution in the nanopore interior is significantly impacted by the bulk concentration. The electric resistances under the negative and positive temperature differences exhibit no obvious difference due to equivalent average temperature. Based on the system's temperature response at low bulk concentrations, a tunable ionic current source can be established with asymmetric temperatures employed. As shown in Fig. 8, the streaming current is tuned by the reservoir temperature at the exit side while the electric resistance is determined by the reservoir temperature at the entrance side.

As shown in Fig. 9, at low membrane thermal conductivities, the IICP is formed in the nanopore interior. The negative temperature difference induces the IICP in the nanopore interior, generating a co-flow concentration gradient that augments the streaming current and the power output. The IICP induced under the positive temperature difference generates a co-flow concentration gradient, which is adverse to the power enhancement. Therefore, electric power enhancement under the negative temperature difference overrides that under the positive temperature difference. A large membrane thermal conductivity vanishes the IICP in the nanopore interior while it induces EICP in the solution reservoirs near the nanopore ends. The EICP is enhanced under the negative temperature difference and is suppressed under the positive one due to the Soret effect, resulting in more significant electric power improvement under the positive temperature difference. At a bulk concentration of 1 mM, the electric power under the positive temperature difference is 10.01 % larger than that under the negative temperature difference for the membrane thermal conductivity at 30 W·m^{-1}K^{-1}. More details about the electric power under different bulk concentrations and asymmetric temperature difference can be seen in Fig. A5 in the Appendix.

Fig. 10 shows the impact of the channel radius on the EKEC performance with asymmetric temperature difference employed. Under different operating temperature configurations, all the current and electric power increases with increasing channel radius for larger channel radius contributes to larger streaming flowrate under the specific pressure difference applied. As mentioned above, at small membrane thermal conductivities, a negative temperature difference contributes more to the electric power due to the IICP in the nanopore interior. At large membrane thermal conductivities, due to the impact of EICP, the electric power under the positive temperature difference is larger than that under the negative temperature difference.

In the transmembrane flow direction, the largest steric hindrance lies in the suddenly shrunken nanopore entrance. When temperature difference employed across the membrane, obviously enhanced streaming flow is observed due to decreased viscosity (Fig. A4 in the in the Appendix). The streaming flowrate under the negative and positive temperature differences does not present significant obviously difference. As shown in Fig. 11, due to the compromise between the electric power and power consumption with asymmetric temperature difference applied, the energy efficiency decreases with increasing thermal conductivities under the negative temperature difference while it increases under the positive temperature difference. With increasing thermal conductivities, the energy efficiency under the negative temperature difference shifts from promotion to inhibition, and energy efficiency shifts from inhibition to promotion under the negative temperature. At a bulk concentration of 1 mM at k = 0.15 W•m^{-1}K^{-1}, the energy conversion efficiency is augmented by 30.3 % under the negative temperature difference, and is decreased by 57.2 % under the positive temperature difference. At k = 120 W•m^{-1}K^{-1}, the energy conversion efficiency is decreased by 3.4 % under the negative temperature difference, and is increased by 10.3 % under the positive temperature difference. More details about the energy efficiency under different bulk concentrations and asymmetric temperature difference can be seen in Fig. A6 in the Appendix.

As additional remarks, in calculating the energy efficiency, the transmembrane heat flux is not considered, which could significantly decrease the energy efficiency. Vast amount of waste heat is

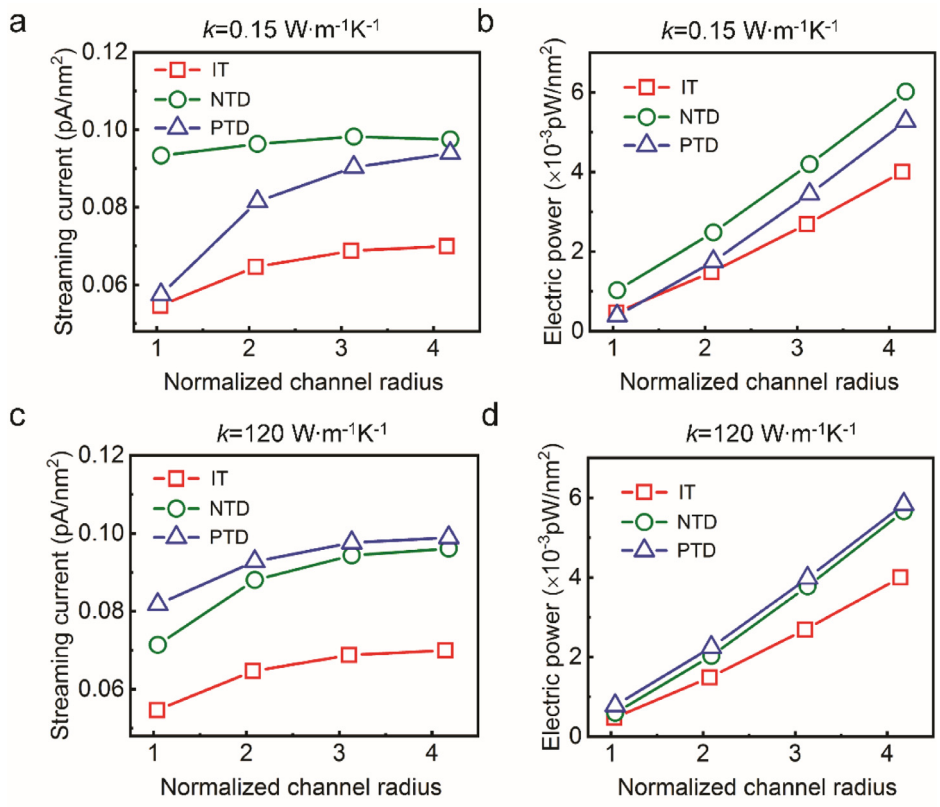

Fig. 10. (a,c) Streaming current, (b,d) electric power under different channel radius. The streaming current and the electric power are normalized by the cross sectional area. The channel radius is normalazed by the Debye length. In the calcualtion, the bulk concentration is 1 mM.

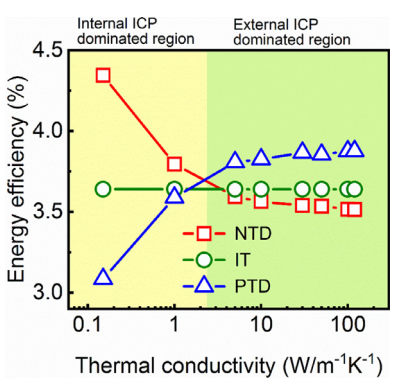

Fig. 11. Energy efficiency with different thermal conductivities at the bulk concentration of 1 mM. In the calculation, the channel radius is 20nm.

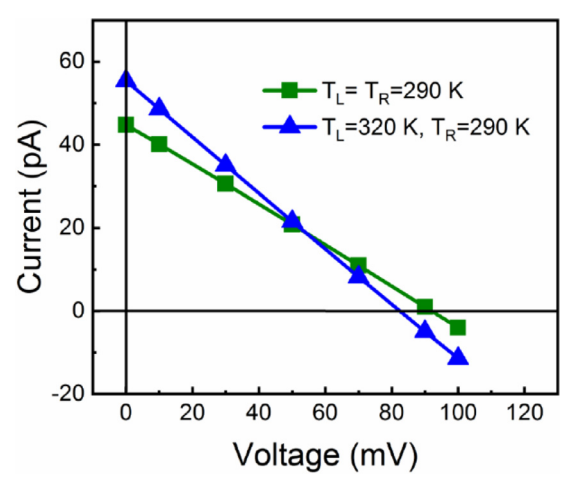

Fig. A1. *I-V* curves under under the isothermal and non-isothermal conditions. In the calculation, the bulk concentration is 1 mM. The membrane material is chosen as PET with the thermal conductivity of k=0.15 W•m^{-1}K^{-1}. In the calculation, the channel radius is 20nm.

produced in the industrial and human activities. Over 60% of the waste heat belongs to low-grade waste heat with the temperature below 100 °C [45]. Small temperature difference above the environment hinders effective utilization of the low temperature waste heat with satisfied energy efficiency via existing commercial technologies [46]. Efficient utilization such waste heat could alleviate the issue induced by increasing energy demand, such as environmental pollution and global warming. The operating temperature of the electrokinetic energy conversion process can be controlled using such waste heat. Heat exchangers can be installed to heat one side of the salt solutions in the electrokinetic energy conversion process, forming a transmembrane temperature, thus to offer an upgraded power output. To enhance the electric power and provide a high ionic flux, for membranes with small membrane thermal conductivities, a negative temperature difference is preferred; for membranes with large thermal conductivities, a positive temperature difference is more promising. For an experimental guide, the asymmetric temperature difference could be constructed by water-bath heating or far infrared heating at one side of the solution reservoirs.

4. Conclusion

In present study, the effects of temperature and membrane thermal conductivity on the EKEC performance are systematically investigated. Under isothermal conditions, elevated temperature can improve the streaming potential while it could not augment the energy efficiency. Under non-isothermal conditions, at small membrane thermal conductivities, a negative temperature difference contributes to the electric power for dramatically enhanced streaming current for enhanced ion mobility along the streaming direction induces an internal ion concentration polarization (IICP) that generates a co-flow concentration gradient in the nanopore interior. At large membrane thermal conductivities, a positive temperature difference reverses the external ion concentration polarization (EICP) in the solution reservoirs due to the Soret effect, resulting in more obvious electric power improvement than that under the negative temperature difference. At a bulk concentration of 1 mM, the electric power under the positive temperature difference is 10.01 % larger than that under the negative temperature difference for the membrane thermal conductivity at 30 $W \cdot m^{-1}K^{-1}$. In addition, a criterion to enhance the EKEC performance via employing asymmetric temperatures is proposed, and a simple way to construct a tunable ionic current source is presented. Present study provides guidance for enhancing the EKEC performance by employing waste heat, and fabricating nanofluidic functional devices.

Author Statement

Rui Long: Conceptualization, Writing- Original draft. **Fan Wu**: Visualization, Investigation. **Xiyu Chen**: Formal analysis. **Zhichun Liu**: Conceptualization. **Wei Liu**: Writing - Review & Editing.

Declaration of Competing Interest

The authors declared that they have no conflicts of interest to this work.

Acknowledgements

This work was financially supported by the National Natural Science Foundation of China (51706076, 51736004).

Appendix

A1. Temperature-depended properties

The temperature dependence of relative permitivity (ε_r) is [33]

$$\varepsilon_r = \exp(4.47615 - 4.60128 \times 10^{-3}\Delta T + 2.6952 \times 10^{-7}(\Delta T)^2) \tag{A1}$$

where $\Delta T = T - 273.15$, $0 \le \Delta T \le 100$.

The temperature dependence of the viscosity is [37]

$$\mu = 2.414 \times 10^{-5} \times 10^{247.8/(T-140)},\ 273.15 \le T \le 643.15 \tag{A2}$$

Based on the Nernst-Haskell equation, the diffusive coefficient D_i ($i = 1$ for K^+ and $i = 2$) for Cl^-) [37]

$$D_i = \frac{RT}{F^2}\left[\frac{1/|z_i|}{1/\lambda_i^0}\right] \tag{A3}$$

where the λ_i^0 is the temperature depended limiting conductance of the ith ionic species.

A2. I-V *curves and electric resistance*

The *I-V* curves of the nanofluidic electrokinetic energy conversion system for a PET membrane (k = 0.15 $W \bullet m^{-1}K^{-1}$) under the isothermal and non-isothermal conditions are presented in FigureA1. The nanofluidic power generation system exhibits Ohm like behavior: the ionic current presents a linear relationship with voltages. Therefore, the electric resistance can be obtained by the calculating the slop of the *I-V* curve through linear fitting from calculated currents under different applied voltages.

A3. Temperature profiles

Temperature profiles under the negative and positive temperature differences for various membrane thermal conductivities at the bulk concentration of 1 mM are plotted in Fig. A2. At small membrane thermal conductivities, significant temperature gradient exists in the nanopore interior, and the temperature gradient in reservior temperature is relatively small. At large membrane thermal conductivities, the temperature gradient in the nanopre interior vanishes, while significant temperature gradient exists in the reserviors.

A4. Cation concentration profiles

Fig. A3 shows the concentration profiles under various membrane thermal conductivities at the large bulk concentration. The EDL overlapping degree is much less, and the ion concentration in the nanopore interior is significantly impacted by the bulk concentration. At large membrane conductivities, a reversed external ion concentration polarization (EICP) occurs, which leads to aggreagration/depletion at the entrance/exit side in the reserviors under the positive temperature difference, generating a co-flow concentration gradient that contributes to the streaming current. A negative temperature difference leads to depletion/aggreagration at the entrance/exit side in the reserviors, generating a counter-flow concentration gradient that hinders the streaming current.

A5. Streaming flowrate

The streaming flowrate under various membrane thermal conductivities and bulk concentrations is depicted in Fig. A4. When temperature difference employed across the membrane, obviously enhanced streaming flow is observed. The streaming flowrate under the negative and positive temperature differences does not present significant obviously difference.

A5. Electric power

Fig. A5 shows under asymmetric temperature difference. At low membrane thermal conductivities, electric power enhancement under the negative temperature difference overrides that under the positive temperature difference. At large membrane thermal conductivities, more significant electric power improvement is observed under the positive temperature difference.

A6. Energy efficiency

As shown in Fig. A6, under small thermal conductivities, a positive temperature difference suppresses the energy efficiency due to significantly enhanced power consumption. At larger thermal conductivities, the energy efficiency under the positive temperature difference is larger than that under the negative temperature difference.

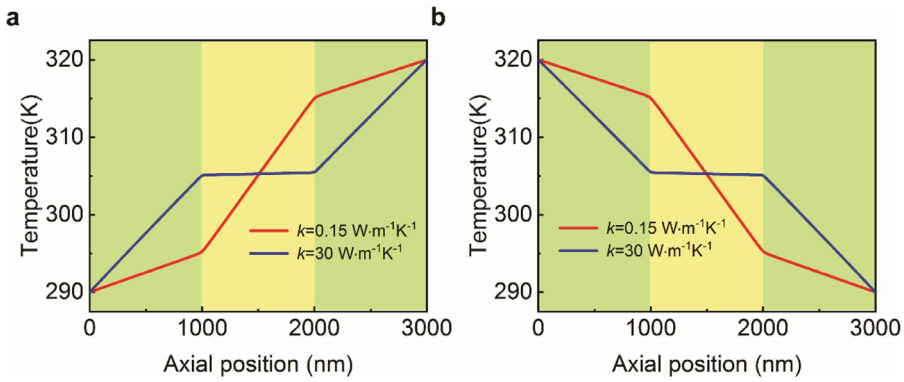

Fig. A2. Temperature profiles under the (a) and (b) PTD for various membrane thermal conductivities. In the calculation, the channel radius is 20nm and the bulk concentration is 1 mM.

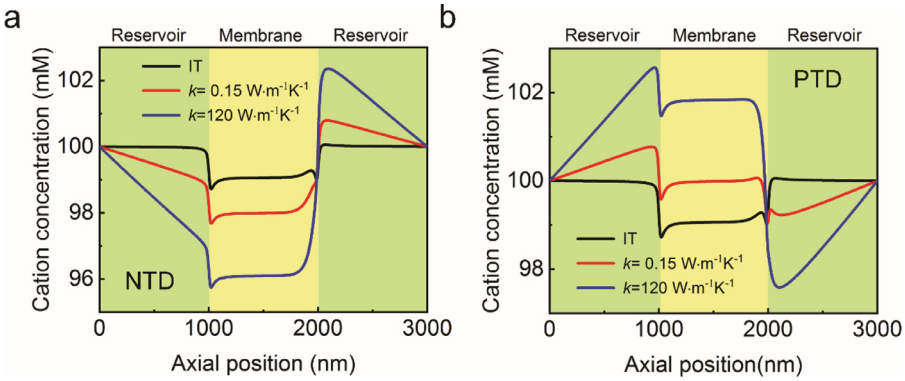

Fig. A3. Cation concentration profiles for various membrane thermal conductivities. (a) under the NTD; (b) under the PTD. In the calculation, the channel radius is 20nm and bulk concentration of 100 mM.

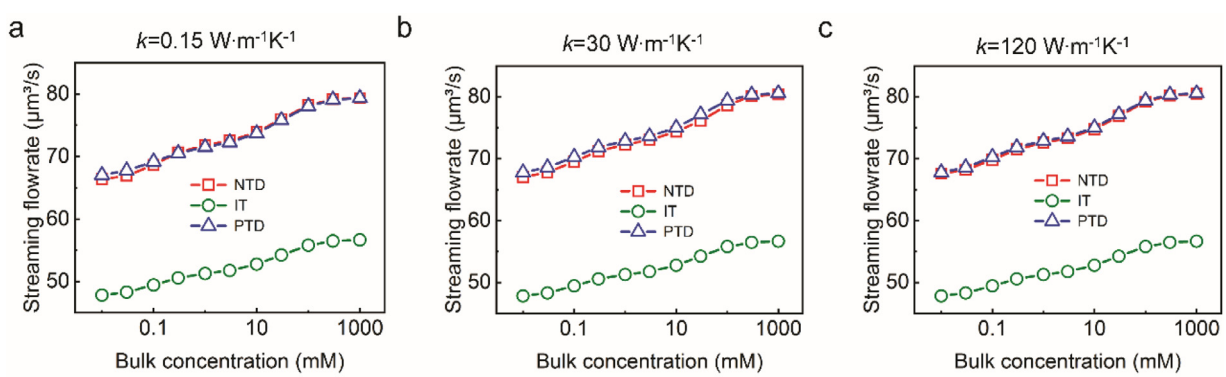

Fig. A4. Streaming flowrate under various thermal conductivities, (a) k=0.15 W•m^{-1}K^{-1}; (b) k=30 W•m^{-1}K^{-1}; (c) k=120 W•m^{-1}K^{-1}. In the calculation, the channel radius is 20nm.

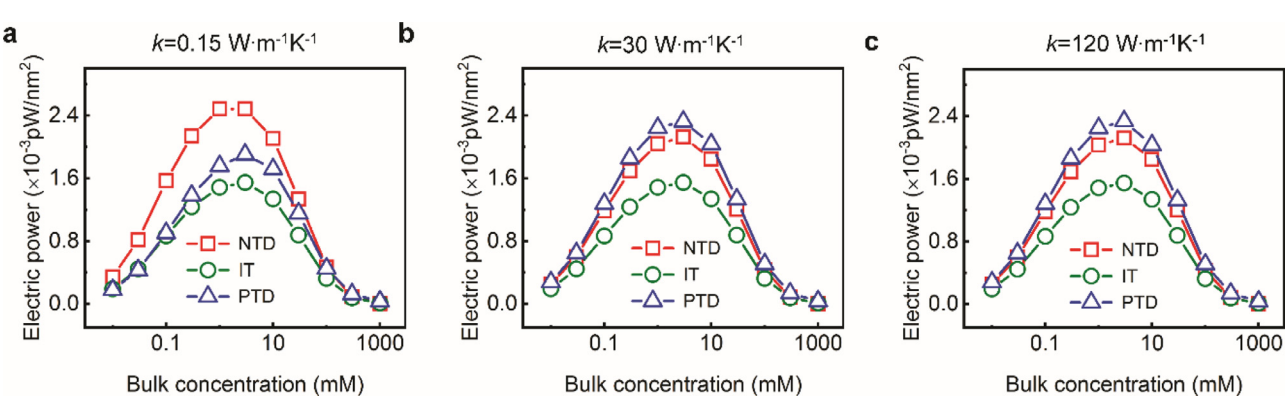

Fig. A5. Electric power under asymmetric temperature difference. (a) k=0.15 W•m^{-1}K^{-1}; (b) k=30 W•m^{-1}K^{-1}; (c) k=120 W•m^{-1}K^{-1}. The electric power is normalized by the cross sectional area. In the calculation, the channel radius is 20nm.

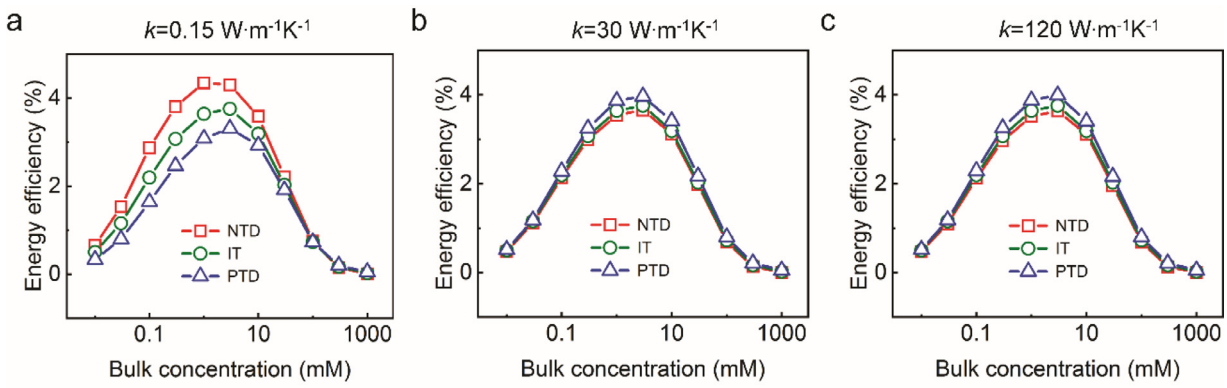

Fig. A6. Energy efficiency under asymmetric temperature difference. (a) k=0.15 W•m^{-1}K^{-1}; (b) k=30 W•m^{-1}K^{-1}; (c) k=120 W•m^{-1}K^{-1}. In the calculation, the channel radius is 20nm.

References

[1] W. Zhang, Q. Wang, M. Zeng, C. Zhao, Thermoelectric effect and temperature–gradient-driven electrokinetic flow of electrolyte solutions in charged nanocapillaries, Int. J. Heat Mass Transf. 143 (2019) 118569.

[2] C. Qi, C.-O. Ng, Electroosmotic flow of a two-layer fluid in a slit channel with gradually varying wall shape and zeta potential, Int. J. Heat Mass Transf. 119 (2018) 52–64.

[3] D. Maynes, B.W. Webb, The effect of viscous dissipation in thermally fully-developed electro-osmotic heat transfer in microchannels, Int. J. Heat Mass Transf. 47 (2004) 987–999.

[4] X. Xuan, D. Sinton, D. Li, Thermal end effects on electroosmotic flow in a capillary, Int. J. Heat Mass Transf. 47 (2004) 3145–3157.

[5] S. Majumder, J. Dhar, S. Chakraborty, Resolving anomalies in predicting electrokinetic energy conversion efficiencies of nanofluidic devices, Sci. Rep. 5 (2015) 14725.

[6] H.-C. Chang, G. Yossifon, E.A. Demekhin, Nanoscale electrokinetics and microvortices: how microhydrodynamics affects nanofluidic ion flux, Annu. Rev. Fluid Mech. 44 (2012) 401–426.

[7] A. Bentien, T. Okada, S. Kjelstrup, Evaluation of nanoporous polymer membranes for electrokinetic energy conversion in power applications, J. Phys. Chem. C. 117 (2013) 1582–1588.

[8] C.C. Chang, R.J. Yang, Electrokinetic energy conversion in micrometer-length nanofluidic channels, Microfluid. Nanofluidics. 9 (2010) 225–241.

[9] F.H.J. Van Der Heyden, D.J. Bonthuis, D. Stein, C. Meyer, C. Dekker, Power generation by pressure-driven transport of ions in nanofluidic channels, Nano Lett. 7 (2007) 1022–1025.

[10] A. Mansouri, S. Bhattacharjee, L.W. Kostiuk, Electrokinetic energy conversion by microchannel array: Electrical analogy, experiments, and electrode polarization, J. Phys. Chem. C. 118 (2014) 24310–24324.

[11] Y. Liu, Y. Jian, C. Yang, Electrochemomechanical energy conversion efficiency in curved rectangular nanochannels, Energy 198 (2020) 117401.

[12] A. Bandopadhyay, S. Chakraborty, Steric-effect induced alterations in streaming potential and energy transfer efficiency of non-newtonian fluids in narrow confinements, Langmuir 27 (2011) 12243–12252.

[13] M. Reshadi, M.H. Saidi, The role of ion partitioning in electrohydrodynamic characteristics of soft nanofluidics: inclusion of EDL overlap and steric effects, Chem. Eng. Sci. 190 (2018) 443–458.

[14] A. Alizadeh, M.E. Warkiani, M. Wang, Manipulating electrokinetic conductance of nanofluidic channel by varying inlet pH of solution, Microfluid. Nanofluidics. 21 (2017) 52.

[15] X. Hu, X. Kong, D. Lu, J. Wu, A molecular theory for predicting the thermodynamic efficiency of electrokinetic energy conversion in slit nanochannels, J. Chem. Phys. 148 (2018) 084701.

[16] A. Poddar, D. Maity, A. Bandopadhyay, S. Chakraborty, Electrokinetics in polyelectrolyte grafted nanofluidic channels modulated by the ion partitioning effect, Soft Matter 12 (2016) 5968–5978.

[17] H. Cheng, Y. Zhou, Y. Feng, W. Geng, Q. Liu, W. Guo, L. Jiang, Electrokinetic energy conversion in self-assembled 2D nanofluidic channels with janus nanobuilding blocks, Adv. Mater. 29 (2017) 1700177.

[18] Y. Zhang, Y. He, M. Tsutsui, X.S. Miao, M. Taniguchi, Short channel effects on electrokinetic energy conversion in solid-state nanopores, Sci. Rep. 7 (2017) 1–14.

[19] L. Jubin, A. Poggioli, A. Siria, L. Bocquet, Dramatic pressure-sensitive ion conduction in conical nanopores, Proc. Natl. Acad. Sci. 115 (2018) 4063–4068.

[20] R. Saini, A. Garg, D.P.J. Barz, Streaming potential revisited: the influence of convection on the surface conductivity, Langmuir 30 (2014) 10950–10961.

[21] Y. Xie, X. Wang, J. Xue, K. Jin, L. Chen, Y. Wang, Electric energy generation in single track-etched nanopores, Appl. Phys. Lett. 93 (2008) 163116.

[22] H. Zhao, Streaming potential generated by a pressure-driven flow over superhydrophobic stripes, Phys. Fluids. 23 (2011) 022003, doi:10.1063/1.3551616.

[23] M. Malekidelarestaqi, A. Mansouri, S.F. Chini, Electrokinetic energy conversion in a finite length superhydrophobic microchannel, Chem. Phys. Lett. 703 (2018) 72–79.

[24] H.F. Huang, P.W. Yang, Electrokinetic streaming power generation using squeezing liquid flows in slit channels with wall slip, Colloids Surfaces A Physicochem. Eng. Asp. 514 (2017) 192–208.

[25] B. Fan, P.R. Bandaru, Modulation of the streaming potential and slip characteristics in electrolyte flow over liquid-filled surfaces, Langmuir 35 (2019) 6203–6210.

[26] Y. Yan, Q. Sheng, C. Wang, J. Xue, H.C. Chang, Energy conversion efficiency of nanofluidic batteries: hydrodynamic slip and access resistance, J. Phys. Chem. C. 117 (2013) 8050–8061.

[27] C.C. Chang, R.J. Yang, Electrokinetic energy conversion efficiency in ion-selective nanopores, Appl. Phys. Lett. 99 (2011) 083102.

[28] L. Mei, L.-H. Yeh, S. Qian, Buffer anions can enormously enhance the electrokinetic energy conversion in nanofluidics with highly overlapped double layers, Nano Energy 32 (2017) 374–381.

[29] D.N. Østedgaard-Munck, J. Catalano, M.B. Kristensen, A. Bentien, Membrane-based electrokinetic energy conversion, Mater. Today Energy. 5 (2017) 118–125.

[30] K. Liu, T. Ding, X. Mo, Q. Chen, P. Yang, J. Li, W. Xie, Y. Zhou, J. Zhou, Flexible microfluidics nanogenerator based on the electrokinetic conversion, Nano Energy 30 (2016) 684–690.

[31] S. Haldrup, J. Catalano, M. Hinge, G.V. Jensen, J.S. Pedersen, A. Bentien, Tailoring membrane nanostructure and charge density for high electrokinetic energy conversion efficiency, ACS Nano 10 (2016) 2415–2423.

[32] S. Haldrup, J. Catalano, M.R. Hansen, M. Wagner, G.V. Jensen, J.S. Pedersen, A. Bentien, High electrokinetic energy conversion efficiency in charged nanoporous nitrocellulose/sulfonated polystyrene membranes, Nano Lett. 15 (2015) 1158–1165.

[33] A. Würger, A. Wu, Transport in charged colloids driven by thermoelectricity, Phys. Rev. Lett. 101 (2008) 5–8, doi:10.1103/PhysRevLett.101.108302.

[34] D. Vigolo, R. Rusconi, H.A. Stone, R. Piazza, Thermophoresis: microfluidics characterization and separation, Soft Matter 6 (2010) 3489–3493.

[35] J.A. Wood, A.M. Benneker, R.G.H. Lammertink, Temperature effects on the electrohydrodynamic and electrokinetic behaviour of ion-selective nanochannels, J. Phys. Condens. Matter. 28 (2016) 114002.

[36] R. Long, Z. Kuang, Z. Liu, W. Liu, Temperature regulated reverse electrodialysis in charged nanopores, J. Memb. Sci. 561 (2018) 1–9.

[37] R. Long, Z. Kuang, Z. Liu, W. Liu, Ionic thermal up-diffusion in nanofluidic salinity-gradient energy harvesting, Natl. Sci. Rev. 6 (2019) 1266–1273.

[38] A.M. Benneker, H.D. Wendt, R.G.H. Lammertink, J.A. Wood, Influence of temperature gradients on charge transport in asymmetric nanochannels, Phys. Chem. Chem. Phys. 19 (2017) 28232–28238.

[39] H. Chen, V.V Ginzburg, J. Yang, Y. Yang, W. Liu, Y. Huang, L. Du, B. Chen, Thermal conductivity of polymer-based composites: fundamentals and applications, Prog. Polym. Sci. 59 (2016) 41–85.

[40] R. Long, Z. Luo, Z. Kuang, Z. Liu, W. Liu, Effects of heat transfer and the membrane thermal conductivity on the thermally nanofluidic salinity gradient energy conversion, Nano Energy 67 (2020) 104284.

[41] V.-P. Mai, R.-J. Yang, Boosting power generation from salinity gradient on high--density nanoporous membrane using thermal effect, Appl. Energy 274 (2020) 115294.

[42] T. Ghonge, J. Chakraborty, R. Dey, S. Chakraborty, Electrohydrodynamics within the electrical double layer in the presence of finite temperature gradients, Phys. Rev. E. 88 (2013) 053020.

[43] D. Vigolo, S. Buzzaccaro, R. Piazza, Thermophoresis and thermoelectricity in surfactant solutions, Langmuir 26 (2010) 7792–7801.
[44] Y. Ai, M.K. Zhang, S.W. Joo, M.A. Cheney, S.Z. Qian, Effects of electroosmotic flow on ionic current rectification in conical nanopores, J. Phys. Chem. C. 114 (2010) 3883–3890.
[45] C. Forman, I.K. Muritala, R. Pardemann, B. Meyer, Estimating the global waste heat potential, Renew. Sustain. Energy Rev. 57 (2016) 1568–1579.
[46] R. Long, B. Li, Z. Liu, W. Liu, Hybrid membrane distillation-reverse electrodialysis electricity generation system to harvest low-grade thermal energy, J. Memb. Sci. 525 (2017) 107–115.